

Supporting information:

In this section additional information is given about:

- Pilot plant for steam cracking
- Detailed decoking procedure of the steam cracking reactor
- Comprehensive 2D GC analysis of the obtained products and the used GC×GC settings
- The single event microkinetic model for steam cracking of the HDO feed
- Furnace simulation
- Economic analysis
- List of abbreviations

Pilot plant for Steam cracking

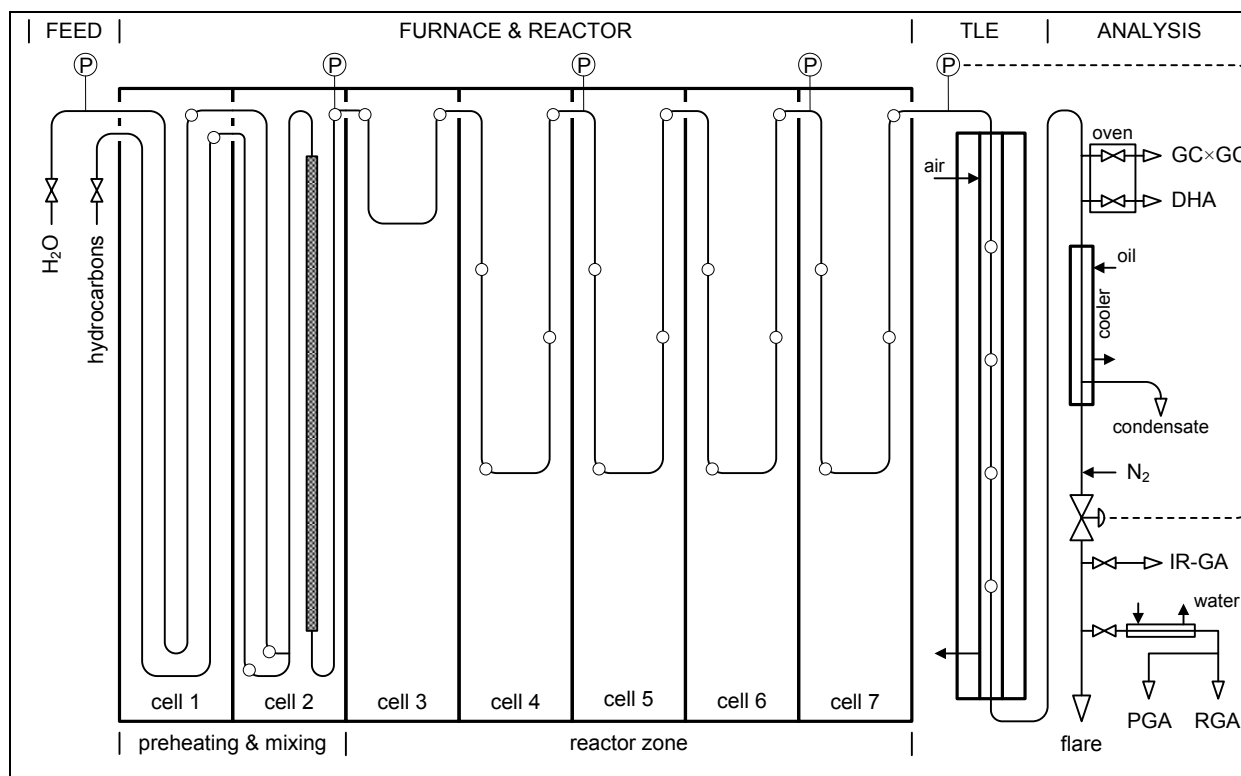


Figure 1: Schematic overview of the pilot plant setup, indicating the most important process gas temperature (\circ) and pressure measurements (P)

The steam cracking pilot plant unit has been extensively described in previous papers by Dhuyvetter et al.¹ and Wang et al.². A schematic representation of the pilot plant units is given in Figure 1. The furnace, built of silica/alumina brick (Li23), is 4 m long, 0.7 m wide and 2.6 m high. It is fired by means of 90 premixed gas burners, mounted with automatic fire checks arranged on the side walls in such a way as to provide a uniform distribution of heat. The fuel supply system comprises a combustion controller for the regulation of the fuel-to-air ratio and the usual safety devices. The furnace is divided into seven separate cells that can be fired independently so that any type of temperature profile can be set easily. In this study, the cracking coil is made of Incoloy 800HT. It is 12.8 m long and has an internal diameter of 9 mm. These dimensions are chosen to achieve turbulent flow conditions in the coil with reasonable feed flow rates. Twenty thermocouples and five manometers are mounted along the coil to measure the temperature and pressure of the reacting gas. The pilot plant effluent is sampled on-line, i.e. during pilot plant operation, and at high temperature (400°C-500°C). The complexity of the effluents calls for several analyzers, including an infrared CO/CO₂ gas analyzer (IR-GA) and four gas chromatographs: a permanent gas analyzer (PGA), a refinery gas analyzer (RGA), a detailed hydrocarbon analyzer (DHA) and the GC×GC-FID/TOF-MS.

The analytical equipment is positioned at different positions on the reactor effluent line, as illustrated in Figure 1. Using a valve-based sampling system and a uniformly heated transfer line a gaseous sample of the reactor effluent is injected onto the DHA and/or the GC×GC. The sampling system consists of two high temperature 6-port 2-way valves, kept at 300°C in the so-called sampling oven to prevent condensation of high molecular weight components. As shown by Van Geem et al. ³, the temperature at which sampling occurs is well above the dew point of the effluent sample.

This approach allows analysis of the entire product stream, from methane to PAHs, in a single run of the DHA or GC×GC. The quantification of all pilot plant effluent components, ranging from H₂, CO and methane to PAHs, is done using an internal standard (N₂), a fixed amount of which is continuously added to the product stream, as indicated in Figure 1.

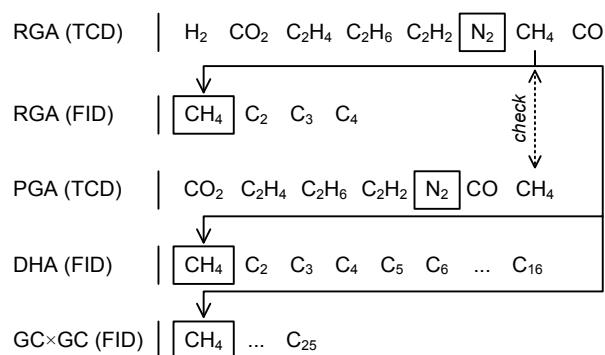


Figure 2: Use of reference components for quantitative on-line effluent analysis

The followed quantification approach is based on multiple reference components, as illustrated in Figure 2, and allows to successfully combine the data from the different instruments. Using the PGA and channel 2 of the RGA, see Figure 2, the amount of methane present in the effluent can be determined based on the known mass flow rate of N₂ and the peak surface areas A_{CH₄} of methane and nitrogen A_{N₂}.

$$\dot{m}_{\text{CH}_4} = \frac{f_{\text{CH}_4} \cdot A_{\text{CH}_4}}{f_{\text{N}_2} \cdot A_{\text{N}_2}} \dot{m}_{\text{N}_2} \quad (1)$$

The response factor of methane is chosen to be unity ($f_{\text{CH}_4} = 1$). The relative response factor for nitrogen is determined by calibration. Subsequently, methane is used as a secondary internal standard for all other quantitative analyses, i.e. the analyses performed on the RGA-FID channel, the DHA and the GC×GC-FID. The flow rates of the other components can hence be calculated according to the following equation:

$$\dot{m}_i = \frac{f_i \cdot A_i}{f_{\text{CH}_4} \cdot A_{\text{CH}_4}} \dot{m}_{\text{CH}_4} \quad (2)$$

For all major components, the relative response factors f_i on each FID detector were determined by calibration. For the minor products theoretical relative response factors permit to determine their absolute mass flow rates⁴.

After cracking, the effluent is quenched in a concentric heat exchanger, in which the process gas can be cooled to 150 °C by means of cooling oil. Before cooling a small fraction of the effluent is sampled for on-line GC and GC×GC analysis. Peak identification and integration are performed using ChromCard. Calculation of the product yields is based on the mass flow rates of the effluent components as described by Van Geem et al.⁵

For the coking experiments identical process conditions are used in the runs performed with (100 ppm DMDS continuously added to the feed) and without additives. During a coking run the conditions are kept fixed for a period of 6 hours. In the radiant coil, cracking and coke deposition are considered to occur only in the cells where $T > 600$ °C, i.e. cells 3 to 7. For the temperature profiles used in this study, the reactor surface area available for coke deposition amounts to 0.34 m². First the cracking coil is heated-up under a steam flow of $1.1 \cdot 10^{-3}$ kg s⁻¹ to the set temperature profile. When the specified temperature profile is reached, the steam flow rate is set to the desired value for cracking and naphtha is introduced. Upon the introduction of naphtha, the temperature in the cracking coil decreases by about 20 °C due to the endothermic nature of the cracking reactions. After about 20 min, the temperature of the

cracking coil returned to the set value. Naphtha is cracked at a COP of 1.7 bar, a COT of 850 °C, and a steam dilution of 0.45 kg steam/kg naphtha.

Decoking procedure of the steam cracking reactor

Decoking of the cracking coil is performed with a steam/air mixture at the conditions specified in Table 1. At the start of the procedure, the cracking coil is heated to 800 °C under a nitrogen flow, and then steam is introduced. After 3 min, the nitrogen flow is stopped, and air is admitted. Once most of the coke is removed, the temperature of the coil is increased to 900 °C. When practically all the coke is burnt off, the steam flow is stopped, and further decoking occurred in air only. The standard decoking time is 6000 s. During decoking, the CO and CO₂ concentration in the effluent is determined by means of infra-red analyzers. The volumetric flow rate of the effluent is measured using a Metal Tube Flowmeter (Brooks, MT3809, 5512/CB 101000A). The concentration of CO and CO₂ and the flow rate of the effluent are automatically recorded every 1 s. These data are used to determine the total amount of coke deposited on the reactor surface.

Table 1: Decoking conditions in the pilot plant set-up

	F _{H2O} (g s ⁻¹)	F _{air} (Nl s ⁻¹)	F _{N2} (Nl s ⁻¹)	T _{out,cell3} (°C)	T _{out,cell4} (°C)	T _{out,cell5} (°C)	T _{out,cell6} (°C)	T _{out,cell7} (°C)
Pre-start	0	0	0.18	750	800	800	800	800
Start	0.28	0.18	0	750	800	800	800	800
CO ₂ <1 mol%	0.28	0.18	0	750	900	900	900	900
CO ₂ <0.1 mol%	0	0.18	0	750	900	900	900	900

Comprehensive 2D GC (GC×GC) analysis and procedures

GC×GC differs from two-dimensional GC, i.e. heart-cutting, since not only a few fractions of the eluent from the first column but the entire sample is separated on two different columns^{6, 7}. Two distinctly different separation columns, based on two statistically independent separation mechanisms, are used. Therefore, the two separations are called orthogonal. The first column contains a non-polar stationary phase (separation based on volatility), and the second column is much shorter and narrower and contains a (medium) polar stationary phase (separation based on analyte-stationary phase interaction). One advantage of orthogonality is that ordered structures for structurally related components show up in the GC×GC chromatograms. Compared to one-dimensional GC, comprehensive GC×GC offers an improved resolution for all the components of interest, without loss of time. The signal-to-noise ratio (and sensitivity) is also significantly enhanced⁸.

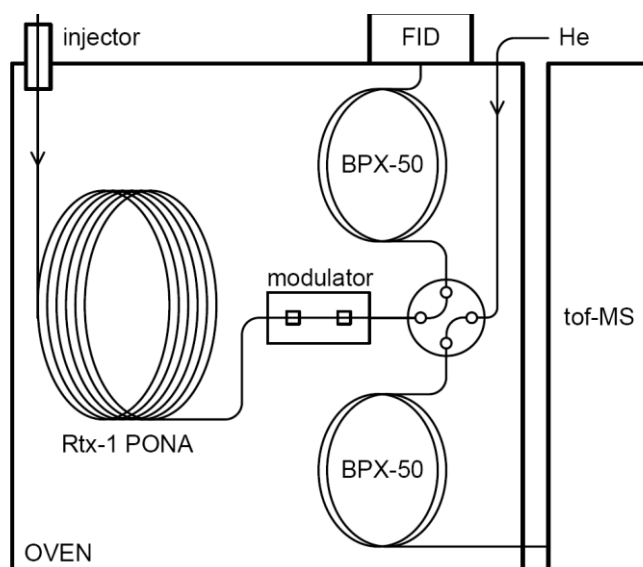


Figure 3: GCxGC set-up with first dimension Rtx-1 PONA column of 50 m and second dimension BPX-50 column of 2m length

Between the two columns an interface, a cryogenic modulator, is present as illustrated in Figure 3. Its main role is to trap adjacent fractions of the analyte eluting from the first-dimension column by cryogenic cooling, and heating-up these cold spots rapidly to release them as refocused analyte pulses onto the second-dimension column. In order to maintain the separation obtained on the first-dimension column, the narrow fractions trapped by the modulator and released on the 2nd column should be no wider than one quarter of the peak widths in the 1st dimension. The term “comprehensive” refers to this aspect of comprehensive GC×GC⁹. As a consequence of this characteristic and since the modulation time must equal

the 2nd dimension run time, second-dimension separations should be very fast, i.e. in the order of 2 to 8 seconds. This will render very narrow 2nd dimension peaks and a demand of correspondingly fast detectors, like a flame ionization detector (FID) or a time-of-flight mass spectrometer (TOF-MS).

A detailed qualitative feedstock characterization is obtained using information from the samples GC×GC-TOF-MS spectrum, the molecular library and the Kovats retention indices. Operation of the GC×GC-TOF-MS is computer controlled, with GC peaks automatically detected as they emerge from the column. Each individual mass spectrum is directly recorded onto the hard disk for subsequent analysis. This technique provides information on the identity of every individual component obtained by chromatographic separation by taking advantage of the common fragmentation pathways for individual substance classes. The interpretation of the mass spectra and library search using the XCalibur software allows the identification of various peaks observed in the chromatogram. The GC×GC settings for analysis of renewable naphtha and the analysis of the cracking effluent are given in Table 2

Table 2: GC×GC settings for off-line and on-line analysis

Detector	FID, 300°C	TOF-MS, 35-400 amu
Injection		
off-line analysis	0.2µl, split flow 150 ml/min, 250°C	
on-line analysis	250 µl (gas), split flow 50 ml/min, 300°C	
Carrier gas	He, constant flow (2.1 ml/min)	He, constant flow (1.8 ml/min)
First column	Rtx-1 PONA ^a (50m×0.25mm×0.5µm)	
Second column	BPX-50 ^b (2m×0.15mm×0.15µm)	
Oven temperature		
off-line analysis	50 → 250°C (3°C/min)	
on-line analysis	-40 (4 min hold) → 40°C (5°C/min) → 300°C (4°C/min)	
Modulation Period		
off-line analysis		4s
on-line analysis		5s

Table 3: GC×GC analysis of HDO-F

C	n-Paraffins	i-Paraffins	Olefins	Naphthenes	Carboxylic acid		SUM
	wt%	wt%	wt%	wt%	wt%		wt%
7	0.004	0.000	0.000	0.000	0.000		0.004
8	0.025	0.000	0.000	0.000	0.000		0.025
9	0.045	0.000	0.000	0.000	0.000		0.045
10	0.119	0.000	0.000	0.004	0.000		0.123
11	0.190	0.000	0.000	0.011	0.000		0.201
12	0.195	0.000	0.000	0.010	0.000		0.204
13	0.200	0.000	0.000	0.015	0.000		0.214
14	0.921	0.010	0.000	0.027	0.000		0.958
15	2.185	0.052	0.000	0.022	0.000		2.260
16	19.625	0.051	0.140	0.008	0.018		19.824
17	6.729	0.219	0.350	0.000	0.000		7.298
18	59.835	0.330	3.861	0.000	0.030		64.026
19	0.504	0.223	0.179	0.000	0.000		0.905
20	0.978	0.216	0.081	0.000	0.000		1.275
21	0.144	0.120	0.000	0.000	0.000		0.264
22	0.273	0.029	0.000	0.000	0.000		0.301
23	0.120	0.071	0.000	0.000	0.000		0.190
24	0.392	0.000	0.000	0.000	0.000		0.392
25	0.135	0.000	0.000	0.000	0.000		0.135
26	0.195	0.000	0.000	0.000	0.000		0.195
27	0.160	0.000	0.000	0.000	0.000		0.160
28	0.291	0.000	0.000	0.000	0.000		0.291
29	0.465	0.000	0.000	0.000	0.000		0.465
30	0.195	0.000	0.000	0.000	0.000		0.195
SUM	93.923	1.321	4.611	0.097	0.048		100.000

Single event microkinetic (SEMK) model for steam cracking of the HD0 feed

Gas-phase pyrolysis of hydrocarbons mainly proceeds through a free-radical mechanism, which is inherently characterized by a vast number of species and reactions. The complexity of such reaction mechanisms increases dramatically as the molar mass of the starting molecule(s) increases. Development of microkinetic models for thermal decomposition of heavier molecules and complex mixtures therefore calls for advanced kinetic modeling tools that: (i) enable automatic generation of the reaction network, (ii) implement a framework for determining reaction rate coefficients and thermodynamic data in a systematic way, (iii) enable to control the complexity of the model in terms of number of species and reactions. Using the procedures discussed concisely below, a SEMK model for steam cracking of hydrodeoxygenated oils, fats and greases was developed. The model presented here includes 233 molecules and 43 radicals in a range of C_0 to C_{26} , as shown in Table 4.

Table 4: Overview of the total number of (pseudo-)components in the SEMK model

Classes of components	Number of (pseudo-)components	Carbon range
molecules	233	$C_0 - C_{26}$
n-paraffins	27	$C_0 - C_{26}$
iso-paraffins ⁽¹⁾	24	$C_4 - C_{26}$
acyclic olefins	129	$C_2 - C_{26}$
cyclic olefins	39	$C_5 - C_{10}$
aromatics	14	$C_6 - C_{14}$
$\beta(\mu)$ radicals⁽²⁾	43	$C_0 - C_7$
Total	276	$C_0 - C_{26}$

⁽¹⁾ After lumping of isomers

⁽²⁾ μ radicals are not explicitly included in the final model by application of the quasi steady state approximation

Reaction network: β and μ network

As shown in Figure 4, the reaction network consists of two parts: the μ network and the β network. The β network is the core of the kinetic model, and contains reactions between smaller (typically C_5 -) molecules, so-called β radicals (R_β) and $\beta\mu$ radicals ($R_{\beta\mu}$). β radicals, such as methyl and hydrogen radicals, are assumed to be only involved in bimolecular reactions, while $\beta\mu$ radicals, e.g. ethyl, vinyl, allyl, etc., are involved in both uni- and

bimolecular reactions. The presented β network contains 1324 reversible elementary reactions: 114 recombination/bond scission reactions, 73 intermolecular addition/ β -scission reactions, 1128 intermolecular hydrogen abstraction reactions, 6 intramolecular hydrogen abstraction reactions (or hydrogen shift reactions), 2 intramolecular addition/ β -scission reactions (or ring closure/ring opening reactions), and 1 (retro-)ene reaction between 51 molecules and 43 $\beta(\mu)$ radicals.

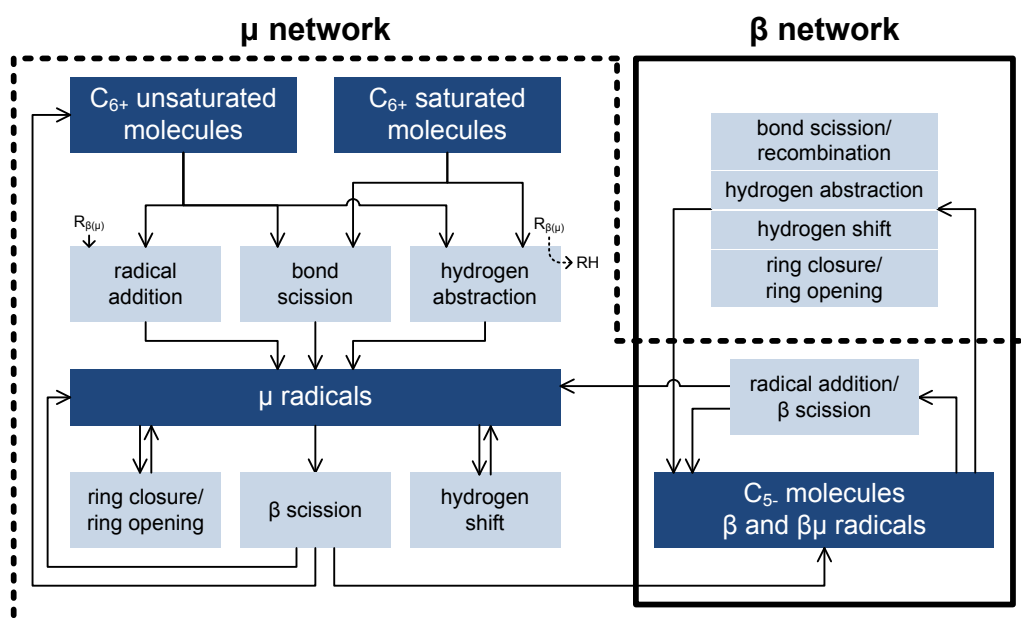


Figure 4: Structure of and reaction families in the single-event microkinetic (SEMK) model – μ network and β network

In contrast to the β network, the μ network is in fact a collection of independent sub-networks that are appended to the β network. Each sub-network is defined by its reactants and by the starting reaction family that transforms these reactants into the initial pool of μ radicals. There are two types of sub-networks, as indicated in Figure 4. The first type contains primary decomposition pathways of larger molecules (typically C_{6+}) starting from hydrogen abstraction, bond scission or radical addition. The latter is only possible when starting molecule is unsaturated. Although not shown in Figure 4, these unsaturated molecules can also undergo retro-ene decomposition, i.e. a concerted pericyclic reaction resulting in smaller unsaturated molecules.

The automatic generation of these sub-networks is made possible by representing molecules and radicals with binary connectivity matrices and manipulation of these matrices to execute reactions and identify products, as first discussed by Clymans and Froment¹⁰. These authors applied the proposed concepts to automatic generation of primary decomposition reactions of

normal and branched paraffins. Later, the computer codes were extended to generate the decomposition pathways of naphthenes and aromatics by Hillewaert et al.¹¹. In this work the decomposition mechanisms of long-chain unsaturated molecules, i.e. the primary decomposition products of all saturated feedstock molecules, have been thoroughly revised. In particular the competition between β scission, hydrogen shift as well as ring closure/ring opening reactions for unsaturated μ radicals is now systematically taken into account. In addition, sub-networks for the secondary hydrocarbon growth, starting from radical additions, have been generated. In total 10114 μ sub-networks were generated. 9159 start from hydrogen abstraction, 415 from bond scission, 451 from radical addition, and 89 from retro-ene decomposition.

Lumping and reduction strategies

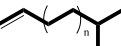
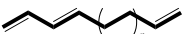
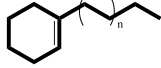
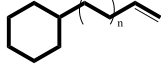
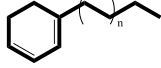
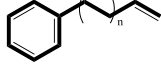
In order to keep the number of species in the final model within limits, three strategies are applied: (i) application of a pseudo-component representation of the feedstock by *a posteriori* lumping, (ii) *in situ* lumping of primary product molecules, and (iii) application of the quasi steady state approximation (QSSA) for μ radicals.

Application of a pseudo-component representation is especially useful when numerous isomers are present in the feed. For example, explicitly accounting for every possible C_{6+} iso-paraffin is basically impossible. However, the reactivity of different isomers can be significantly different and the specific location and number of branches needs to be accounted for during the generation of their μ network decomposition sub-networks. Nevertheless, *a posteriori* lumping (i.e. after network generation) of these sub-networks permits to reduce the number components and consequently the number of continuity equations that has to be accounted for in the final model. For example, the μ network decomposition sub-networks of individual C_{18} iso-paraffins, e.g. 2-methyl-heptadecane, 3-methyl-heptadecane, 2,3-dimethyl-hexadecane, etc., can be conveniently lumped into a single decomposition scheme for the pseudo-component (IPARC18) by imposing a fixed relative abundance of each isomer. Thus, each pseudo-component is defined by its type, e.g. iso-paraffin, and its carbon number, e.g. C_{18} . In principle, the relative abundance of each isomer is different for each feedstock. However, Ranzi et al.¹² showed that the relative abundance of iso-paraffinic isomers in straight-run naphthas is quasi-independent of its source. It is therefore viable to adopt a fixed set of weights per type of feedstock, e.g. straight-run naphtha, FCC naphtha, hydrotreated gas oil, etc. In this work, for hydrodeoxygenated biowaste, decomposition sub-networks for 2-

methyl-, 3-methyl-, 4-methyl, and 2,3-dimethyl alkanes are lumped in a fixed ratio of 45 wt% – 25 wt% – 15 wt% – 15 wt%, based on the feedstock analysis.

Secondly, heavy unsaturated product molecules, i.e. C₇₊ acyclic olefins and C₉₊ cyclic olefins, are lumped *in situ* (i.e. during network generation) into a limited number of pseudo-components, which are again completely defined by a carbon number and a type. For C₇₊ acyclic olefins, a distinction is made between six types of components: α-olefins, other straight chain olefins, branched olefins, straight chain di-olefins, branched di-olefins and tri-olefins. For C₉₊ cyclic olefins a distinction is made between endocyclic olefins, exocyclic olefins, cyclic di-olefins and aromatic olefins. Each type of pseudo-component has been assigned a representative structure as shown in Table 5, which is used to generate μ network sub-networks for their own decomposition.

Table 5: Overview of adopted types of pseudo-component and their representative structure for C₇₊ acyclic olefins and C₉₊ cyclic olefins

Pseudo-component classes of primary products	Representative structure
C₇₊ acyclic olefins	
α-Olefins	
Other straight chain olefins	
Branched olefins	
Straight chain di-olefins	
Branched di-olefins	
Tri-olefins	
C₉₊ cyclic olefins	
Endocyclic mono-olefin	
Exocyclic mono-olefin	
Cyclic di-olefins	
Aromatic olefins	

This lumping strategy results in manageable but sufficiently detailed pseudo-component representation of the heavy unsaturated primary products. In contrast, a much higher level of

detail is taken into account for acyclic olefins with 6 or less carbon atoms and cyclic olefins with 8 or less carbon atoms because of their higher abundance and importance for the formation of aromatics. Finally, note that while the adopted pseudo-component representation is considered suitable to model steam cracking of paraffinic feedstocks, an increased level of detail might be necessary when higher amounts of heavy naphthenes and aromatics are present in the feed.

The final strategy consists of application of the quasi-steady state approximation (QSSA) for μ radicals. In combination with the μ radical hypothesis, application of QSSA to all μ radicals in a certain sub-network results in a set of linear algebraic equations that can be solved during network generation. Doing so, the concentrations of all μ radicals are expressed as a function of the concentrations of the starting reactants of the sub-network. Consequently, the rate-of-production of each molecule and $\beta(\mu)$ radical that is formed in the sub-network is determined by these reactant concentrations only, i.e. not by the concentrations of intermediate μ radicals¹⁰⁻¹⁴. This results in a drastic reduction of the number of species and the number of continuity equations that has to be accounted for in the final model without sacrificing its fundamental nature. In addition, the stiffness of the final set of differential equations is reduced. Table 4 shows that even with the applied lumping and reduction strategies the number of species, and especially the number of olefins in the final model remains quite high. Nevertheless, without these strategies the number of species would be impractically large.

Thermodynamic data

Accurate thermodynamic data is crucial to calculate the rate coefficient of the reverse reactions based on the equilibrium coefficient and the rate coefficient of the forward reaction. Benson's group additive method¹⁵ is widely employed by several stand-alone programs, e.g. THERM¹⁶, THERGAS¹⁷, ThermoDataEstimator (RMG)¹⁸ to automatically calculate standard enthalpies of formation, entropies, and heat capacities. In this work, thermodynamic data of all C₅₊ molecules are determined in the form of NASA polynomials¹⁹, by RMG's ThermoDataEstimator. The thermodynamic data of all C₄ molecules, β radicals and $\beta\mu$ radicals have been determined directly from first principles using the high-accuracy CBS-QB3 compound method with corrections for all internal rotations^{20, 21}. The adopted thermodynamic data of cyclopentadienyl radical was determined by Sharma and Green²².

Kinetic data

On-the-fly group additive calculation of reaction rate coefficients is accomplished by the implementation of a comprehensive framework, which is a consistent extension of Benson's group additivity concept to transition state theory²³⁻²⁸. This framework allows automatic calculation of Arrhenius parameters, and subsequently rate coefficients, using Equations (1)-(3).

$$k(T) = n_e \cdot \tilde{A} \cdot \exp\left(-\frac{E_a}{R \cdot T}\right) \quad (1)$$

$$E_a = E_{a,\text{ref}} + \sum_{i=1}^n \Delta GAV_{E_a,i}^0 \quad (2)$$

$$\log \tilde{A} = \log \tilde{A}_{\text{ref}} + \sum_{i=1}^n \Delta GAV_{\tilde{A},i}^0 \quad (3)$$

All reactions are classified into a limited number of reaction families based on structural similarities of their transition states. The activation energy E_a and the single-event pre-exponential factor \tilde{A} of a certain reaction are obtained by adding contributions to $E_{a,\text{ref}}$ and \tilde{A}_{ref} which are the single-event Arrhenius parameters of the reaction family reference reaction, cfr. Equation (2) and (3). The standard group additive values ΔGAV_i^0 for each of the n contributions depend on the reaction family and account for the structural differences between the transition state of the considered reaction and the reference reaction. The number of contributions equals the number of carbon atoms directly involved in the transition state moiety, i.e. typically 2 or 3. Finally, the reaction rate coefficient is obtained, using Equation (1) in which n_e is the number of single events, i.e. a symmetry contribution that takes into account the internal and external symmetry number and the number of optical isomers of reactants and transition state. This symmetry contribution is not straightforward to calculate automatically, and instead, n_e is approximated by the so-called reaction path degeneracy, i.e. the number of structurally equivalent reaction paths from reactant(s) to products. However, without certain correction factors, this can lead to important discrepancies with the actual number of single-events, i.e. the number of energetically equivalent reaction paths from reactant(s) to transition state. Therefore, based on the extensive set of reactions published by Sabbe et al.²³⁻²⁶, a limited set of correction factors was obtained to improve the automatic calculation of n_e . For example for hydrogen abstractions, the number of single events is the product of the reaction path degeneracy, i.e. the number of structurally equivalent hydrogen

atoms, and a correction factor that depends on the nature of the abstracting radical (e.g. 2 for methyl, 1 for vinylic radicals, 2 for primary radicals, etc.).

The majority of the reference parameters and group additive values have been determined from first principles, and none of the parameters were adjusted to match the experimental data discussed below. The parameters for carbon-centered radical additions and β scissions, hydrogen radical additions and β scissions, hydrogen abstractions by carbon-centered radicals and by hydrogen radicals, retro-ene reactions, ring closure and ring opening reactions were calculated from first principles by Sabbe et al.²³⁻²⁶. In this work, the reported group additive values and the reference parameters calculated at 1000 K are adopted. Currently, no group additive values are available for retro-ene reactions, ring closure and ring opening reactions to take into account structural differences with the reference reaction, and the reference parameters are used in each instance. Parameters for carbon-carbon and carbon-hydrogen radical recombination reactions and the reverse bond scissions were derived from the values calculated by Harding, Klippenstein and Georgievskii²⁹⁻³¹, who combined high-level multi-reference calculations with variable reaction coordinate transition state theory, a variant of energy and angular momentum-resolved variational transition-state theory³². When necessary, the so-called geometric mean rule^{25, 31} was applied to complement the reported kinetic data. The rates for recombination and addition reactions that involve benzyl or cyclopentadienyl radicals were taken from the high temperature combustion mechanism for heavy hydrocarbons (C₁-C₁₆) developed by the CRECK modeling group (POLIMI, Milan, Italy)^{33, 34}. Finally, reference parameters and group additive values for [1.5]- and [1.4]-hydrogen shift reactions are derived from the kinetic data published by Mehl et al.³⁵.

Furnace simulation

For the reactor side the 1 dimensional continuity, momentum and energy equations, resulting in the concentration, temperature and pressure profiles for a given set of process conditions³⁶ are integrated. The steady state continuity equation for a component *j* in the process gas mixture over an infinitesimal volume element with cross sectional surface area Ω , circumference ω and length dz is:

$$\frac{dF_j}{dz} = \left(\sum_{k=1}^{n_r} \nu_{kj} r_k \right) \Omega \quad (4)$$

with F_j the molar flow rate of component *j*, $r_{v,k}$ the reaction rate of reaction *k*, and ν_{kj} the stoichiometric coefficient of component *j*. The energy equation is given by:

$$\sum_j F_j c_{pj} \frac{dT}{dz} = \omega q + \Omega \sum_k r_{v,k} (-\Delta H_k) \quad (5)$$

with q the heat flux to the process gas, c_{pj} the heat capacity of component *j* at temperature *T*, $\Delta_f H_k$ the standard enthalpy of formation of species *k*, $r_{v,k}$ the net production rate for species *k*. The momentum equation accounting for friction and changes in momentum is given by:

$$-\frac{dp_t}{dz} = \alpha \left(\frac{2f}{d_t} + \frac{\zeta}{\pi r_b} \right) \rho_g u^2 + \alpha \rho_g u \frac{du}{dz} \quad (6)$$

with p_t the total pressure, α a conversion factor, f the Fanning friction factor, ρ the density of the gas mixture, r_b the radius of the bend, d_t the diameter and v the velocity. The initial conditions are:

$$T=T_0 \quad C_j=C_{j0} \quad p=p_0 \quad (z=0) \quad (7)$$

If coke formation needs to be accounted for as a function of time and position in the reactor coil, the following continuity equation needs to be added to the set of differential equations:

$$\frac{\partial C_{\text{coke}}}{\partial t} = r_c \quad (8)$$

With r_c the rate of coke formation. The position dependence is obtained through the temperature and partial pressure dependence of the rate of coke formation. At the operating conditions prevailing in industrial cracking units, the largest amount of coke formed during the run length results from the heterogeneous, non-catalytic coke formation³⁷. The model of Reyniers et al.³⁷ allows to simulate the coking rate of heavier feedstocks ranging from light naphtha fractions up to heavy condensates. This model considers 12 reactions in parallel for describing the formation of coke. The rate of coke formation is then expressed as:

$$r_C = C_{H_2} C_{CH_4} \sum_{i=1}^{12} k_i C_i \quad (9)$$

To perform a complete furnace simulation several options exist. In the case Fluent³⁸ is used, then Fluent provides the heat flux profile from simulating the fire box. Another possibility is to obtain the heat flux profile from one of the in house developed software codes FURNACE³⁹ or FLOWSIM⁴⁰. Van Geem et al.⁴¹ showed that the desired reactor outlet conditions (e.g. COT or propene to ethene yield ratio) can also be used as input. In order to solve the resulting two point boundary condition problem, the shooting method⁴² is applied in an iterative procedure. This allows the program to generate the inlet pressure and the heat flux profile corresponding to the requested cracking severity indices at the reactor outlet. This last option is used in the current paper for a naphtha cracking furnace.

Predicting the run length of a furnace requires integrating the full set of differential equations [(4)-(6), (8)]. To do so, the run time is increased in a stepwise manner. Incremental pseudo steady state is assumed for the coking since the main cracking reactions are much faster than the coke formation. This means that the rate of coke formation may be considered constant in each time interval. For the present simulation runtime increments of 100 hours were found to be appropriate. For each time increment a reactor simulation is performed shooting at the specified outlet condition, i.e. a conversion of 99%. The other operating conditions and the furnace characteristics are given in Table 6

Table 6: Furnace, reactor geometry and process conditions for naphtha cracking furnace

Reactor coil	
Type	Split coil
Number of reactors	8
Number of passes	6
Reactor length	53.89 m
Internal reactor diameter (passes 1-4)	0.080 m
External reactor diameter (passes 1-4)	0.096 m
Joining coils before pass 5	2
Internal reactor diameter (passes 5-6)	0.114 m
External reactor diameter (passes 5-6)	0.130 m
Wall thickness	0.008 m
Naphtha flow rate per reactor coil	0.428 kg s ⁻¹
Steam dilution δ	0.70 kg/kg _{HC}
Coil Inlet Temperature (a)	620 °C
Coil Outlet Pressure (b)	1.45 10 ⁵ Pa
Furnace characteristics	
Height	9.09 m

Length	14.40 m
Width	2.50 m
Number of burners	160
Thickness of refractory	0.23 m
Thickness of insulation	0.05 m
Fuel composition	
Methane	95 vol%
Hydrogen	5 vol%
Initial fuel gas flow rate	55 mol s ⁻¹
Air excess	10%
Uniform side wall firing	
Outlet specification	
Feed conversion	99%

Economic analysis

The production cost for high value chemicals (ethene, propene, 1,3-butadiene,...) is of course highly dependent on feedstock prices (both for conventional fossil resources as for the green route). For example during the last half year fossil based naphtha prices have been fluctuating significantly between 900 \$/Mt and 1040 \$/Mt, see Figure A1.

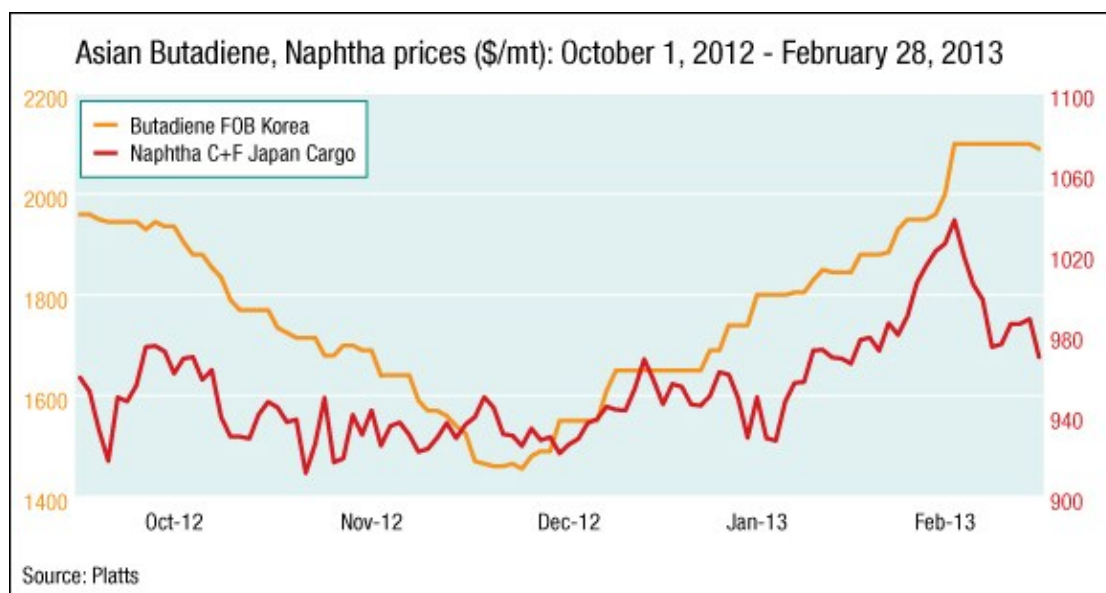


Figure A1: Asian Butadiene and Naphtha prices⁴³

To assess the economic viability of producing green olefins a techno-economic analysis was carried out to retrofit an existing European naphtha cracker.

At the current prices for naphtha (860\$/ton ⁴⁴) and the grease blend (38 cts/lb ⁴⁵) the production cost of the renewable high value chemicals is about 14% higher than for the production out of a conventional naphtha. The higher production cost can be broken down into :

- different feedstock price
- costs of the hydrodeoxygenation (mainly investment and hydrogen consumption)
- different fuel usage (11% lower for the hydrodeoxygenated feed)

However, the higher production cost could be compensated by higher prices for green olefins. According to Brazilian petrochemical company Braskem⁴⁶ green polyethene is a highly valued niche where clients are willing to pay from 20 up to 30% extra compared to traditional polyethene prices.

Prices that were used for this economic analysis are shown in

Table 7. To retrofit an existing naphtha cracker the construction of the pretreater and the hydrotreater are needed in the plant. The investment cost of the pretreater is assumed to be negligible in comparison with the investment cost of the hydrotreater. The production capacity of the hydrotreater is assumed to be around 4000 BPD which is more than enough to supply one oven of the cracker with the HDO-F product. The operating cost of the hydrotreater is based on Pearlson⁴⁷ but since Pearlson includes both a hydrotreater and an isomerization unit the operating costs were assumed to be divided equally among the two units with the exception of the usage of hydrogen of which the costs were completely allocated to the hydrotreater. All costs in Table 7 were recalculated to \$/ton feedstock. To recalculate the investment cost of the hydrocracker the depreciation was scheduled over 10 years. The total production cost on a yearly basis was then calculated using the mass flow rate of a single oven together with the total production of high value chemicals. To make a fair comparison between the cases the total cost was then recalculated based on the amount of high value chemicals products.

Table 7: Investment, feedstock and utility prices for hydrotreater and steam cracker

Feedstocks	
Naphtha (\$/ton)	860 ⁴⁴
Yellow Grease (cts/lb)	38.00 (35.00-40.00) ⁴⁵
Steam cracker utilities	
Fuel gas (\$/Gcal)	21.9 ⁴⁸
Other utilities (\$/ton ethene)	19.4 ⁴⁸
Hydrotreater	
Operating cost (cts/gallon feed)	30
Investment cost (\$)	5.73 MM ⁴⁷

At the current prices of naphtha and the grease blend (Table 7) the production cost of renewable ethene is about 12% higher than that of ethene produced from a conventional naphtha. Since feedstock prices tend to fluctuate over time and because this comparison is very sensitive to feedstock prices two sensitivity analysis's were carried out to see the effect of changing naphtha and feedstock prices. Figure 5 shows the relative cost price for the production of ethene from renewable naphtha when compared to the production from conventional naphtha. In Figure 5 the naphtha price was kept constant at 860 \$/ton while the grease blend price change from 30 to 50 cts/lb. Figure 5 shows that at a very low price of the grease blend (lower than 33 cts/lb) the production of ethene from renewable naphtha's is even cheaper than the production of ethene from conventional naphtha's. When the grease blend price become higher than 45 cts/lb it's more than 30% more expensive to produce ethene from the HDO-F product. At this price the increased price customers pay for green ethene will not be able to compensate the increased cost price and production will be less profitable compared to the production of ethene using a conventional naphtha.

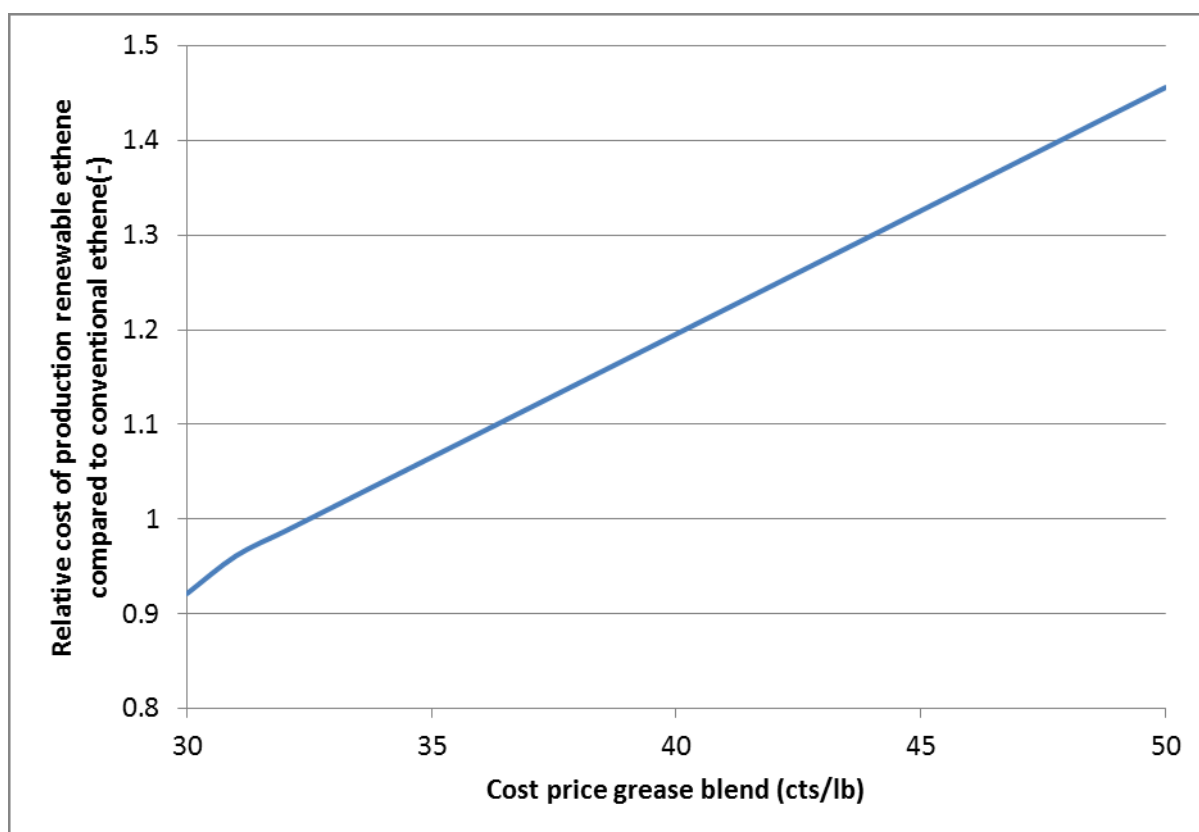


Figure 5: Relative cost price for the production of ethene from renewable naphtha compared to conventional naphtha for varying grease blend prices and at fixed naphtha prices

Figure 6 shows the relative cost price for the production of ethene from renewable naphtha when compared to the production from conventional naphtha. In Figure 6 the grease blend price was kept constant at 38 cts/lb while the naphtha price change from 850 to 1000 \$/ton. Figure 6 shows that the naphtha price needs to increase to 990 \$/ton before the production of ethene out of the HDO-F product becomes cheaper than out of conventional naphtha. When the naphtha prices drop below 750\$/ton the production of ethene from renewable naphtha becomes more than 30% expensive so that the increased cost isn't compensated anymore by the increased selling price for green ethene.

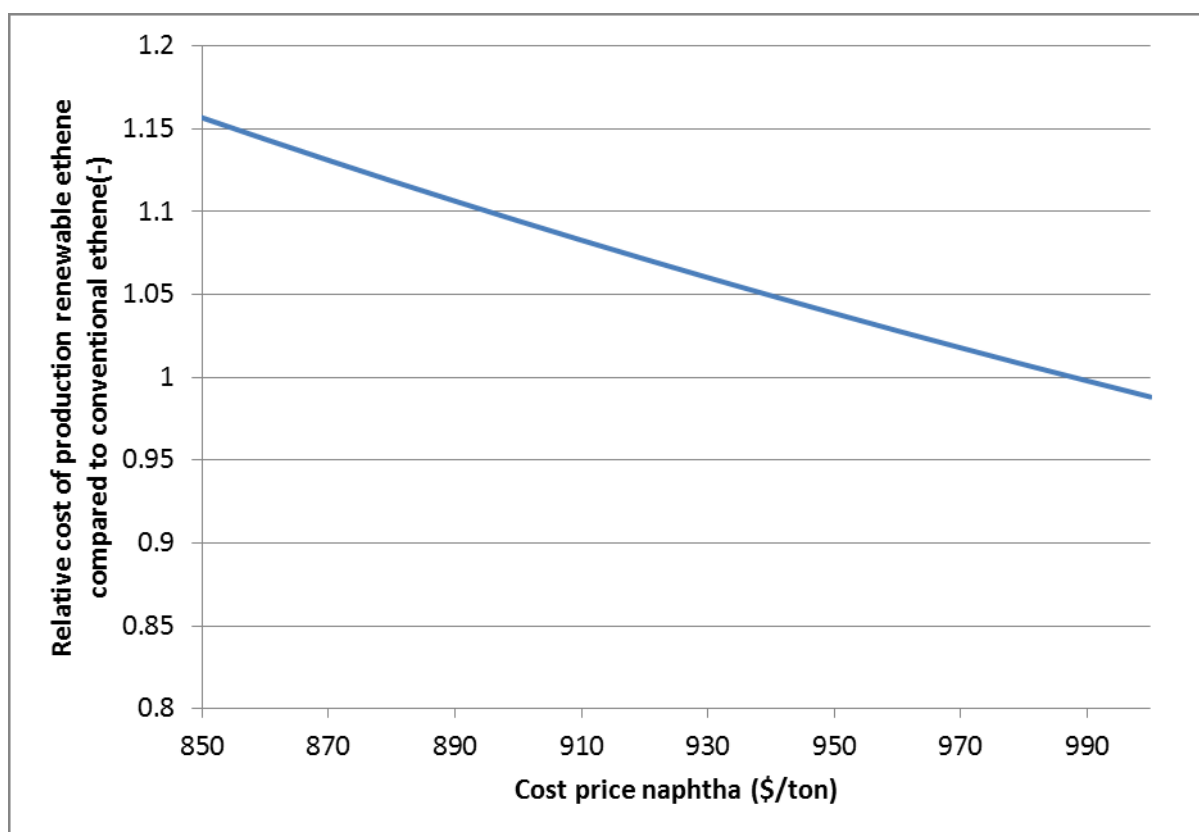


Figure 6: Relative cost price for the production of ethene from renewable naphtha compared to conventional naphtha for varying naphtha prices and at fixed grease blend prices

List of abbreviations

BPD	Barrels per day
BTO	Biomass to Olefins
CIP	Coil inlet pressure
CIT	Coil inlet temperature
COP	Coil outlet pressure
COT	Coil outlet temperature
DHA	Detailed hydrocarbon analyzer
DTO	Distilled tall oil
FCC	Fluid catalytic cracking

FFA	Free fatty acid
FID	Flame ionization detector
F-T	Fischer-Tropsch
GC	Gas chromatography
GC×GC	Comprehensive two-dimensional gas chromatography
HDO	Hydrodeoxygenation
HDO-F	Hydrodeoxygenated feed
HVC	High value chemical
MTO	Methanol to Olefins
P/E	Propene/Ethene
PAH	Polyaromatic hydrocarbon
PGA	Permanent gas analyzer
PINA	Paraffins, Isoparaffins, Naphthenes and aromatics
QSSA	Quasi-steady state approximation
RGA	Refinery gas analyzer
SEMK	Single event microkinetic
TOFA	Tall oil fatty acid
ToF-MS	Time of flight mass spectrometer
δ	Dilution (Flow rate hydrocarbons/Flow rate steam)

References

1. I. Dhuyvetter, M. F. Reyniers, G. F. Froment, G. B. Marin and D. Viennet, *Ind. Eng. Chem. Res.*, 2001, **40**, 4353-4362.
2. J. Wang, M. F. Reyniers and G. B. Marin, *Ind. Eng. Chem. Res.*, 2007, **46**.
3. K. M. Van Geem, I. Dhuyvetter, S. Prokopiev, M. F. Reyniers, D. Viennet and G. B. Marin, *Ind. Eng. Chem. Res.*, 2009, **48**, 10343-10358.
4. J. Beens, H. Boelens, R. Tijssen and J. Blomberg, *HRC J. High Resolut. Chromatogr.*, 1998, **21**, 47-54.
5. K. M. Van Geem, S. P. Pyl, M.-F. Reyniers, J. Vercammen, J. Beens and G. B. Marin, *J. Chromatogr. A*, 2010, **1217**, 6623-6633.
6. J. B. Phillips and J. Z. Xu, *J. Chromatogr. A*, 1995, **703**, 327-334.
7. J. Dalluge, J. Beens and U. A. T. Brinkman, *J. Chromatogr. A*, 2003, **1000**, 69-108.
8. C. Vendeuvre, R. Ruiz-Guerrero, F. Bertoncini, L. Duval and D. Thiebaut, *Oil Gas Sci. Technol.*, 2007, **62**, 43-55.
9. M. Adahchour, J. Beens and U. A. T. Brinkman, *J. Chromatogr. A*, 2008, **1186**.
10. P. J. Clymans and G. F. Froment, *Comput. Chem. Eng.*, 1984, **8**, 137-142.
11. L. P. Hillewaert, J. L. Dierickx and G. F. Froment, *Aiche J.*, 1988, **34**, 17-24.
12. E. Ranzi, M. Dente, A. Goldaniga, G. Bozzano and T. Faravelli, *Prog. Energy Combust. Sci.*, 2001, **27**, 99-139.
13. K. M. Van Geem, M. F. Reyniers and G. B. Marin, *Oil Gas Sci. Technol.*, 2008, **63**, 79-94.
14. M. Dente, G. Bozzano, T. Faravelli, A. Marongiu, S. Pierucci and E. Ranzi, in *Advances in Chemical Engineering*, ed. G. B. Marin, Academic Press, 2007, vol. 32, pp. 51-166.
15. S. W. Benson, *Thermochemical Kinetics: Methods for the Estimation of Thermochemical Data and Rate Parameters*, John Wiley & Sons, New York, 1976.
16. E. R. Ritter and J. W. Bozzelli, *Int. J. Chem. Kinet.*, 1991, **23**, 767-778.
17. C. Muller, V. Michel, G. Scacchi and G. M. Come, *J. Chim. Phys. Phys. - Chim. Biol.*, 1995, **92**, 1154-1178.
18. W. H. Green, J. W. Allen, R. W. Ashcraft, G. J. Beran, C. F. Goldsmith, M. R. Harper, A. Jalan, G. R. Magoon, D. M. Matheu, S. Petway, S. Raman, S. Sharma, K. M. Van Geem, J. Song, J. Wen, R. H. West, A. Wong, H.-W. Wong, P. E. Yelvington and Y. J., RMG - Reaction Mechanism Generator v3.3, <http://rmg.sourceforge.net/>.
19. S. Gordon and B. J. McBride, *Computer program for calculation of complex chemical equilibrium compositions rocket performance incident and reflected shocks, and Chapman-Jouguet detonations*, NASA, Lewis Research Center, Cleveland (OH), USA 1971.
20. M. K. Sabbe, F. De Vleeschouwer, M. F. Reyniers, M. Waroquier and G. B. Marin, *J. Phys. Chem. A*, 2008, **112**, 12235-12251.
21. M. K. Sabbe, M. Saeys, M. F. Reyniers, G. B. Marin, V. Van Speybroeck and M. Waroquier, *J. Phys. Chem. A*, 2005, **109**, 7466-7480.
22. S. Sharma and W. H. Green, *J. Phys. Chem. A*, 2009, **113**, 8871-8882.
23. M. K. Sabbe, M. F. Reyniers, V. Van Speybroeck, M. Waroquier and G. B. Marin, *ChemPhysChem*, 2008, **9**, 124-140.
24. M. K. Sabbe, M. F. Reyniers, M. Waroquier and G. B. Marin, *ChemPhysChem*, 2010, **11**, 195-210.

25. M. K. Sabbe, K. M. Van Geem, M.-F. Reyniers and G. B. Marin, *Aiche J.*, 2011, **57**, 482-496.
26. M. K. Sabbe, A. G. Vandeputte, M. F. Reyniers, M. Waroquier and G. B. Marin, *PCCP*, 2010, **12**, 1278-1298.
27. M. Saeys, M. F. Reyniers, G. B. Marin, V. Van Speybroeck and M. Waroquier, *Aiche J.*, 2004, **50**, 426-444.
28. M. Saeys, M. F. Reyniers, V. Van Speybroeck, M. Waroquier and G. B. Marin, *ChemPhysChem*, 2006, **7**, 188-199.
29. L. B. Harding, Y. Georgievskii and S. J. Klippenstein, *J. Phys. Chem. A*, 2005, **109**, 4646-4656.
30. L. B. Harding, S. J. Klippenstein and Y. Georgievskii, *J. Phys. Chem. A*, 2007, **111**, 3789-3801.
31. S. J. Klippenstein, Y. Georgievskii and L. B. Harding, *PCCP*, 2006, **8**, 1133-1147.
32. Y. Georgievskii and S. J. Klippenstein, *J. Chem. Phys.*, 2003, **118**, 5442-5455.
33. E. Ranzi, A. Frassoldati, T. Faravelli and A. Cuoci, CRECK modeling group - kinetic models, <http://creckmodeling.chem.polimi.it/kinetic.html>.
34. C. Cavallotti, D. Polino, A. Frassoldati and E. Ranzi, *J. Phys. Chem. A*, 2012, **116**, 3313-3324.
35. M. Mehl, G. Vanhove, W. J. Pitz and E. Ranzi, *Combust. Flame*, 2008, **155**, 756-772.
36. K. M. Van Geem, R. Zajdlik, M. F. Reyniers and G. B. Marin, *Chem. Eng. J.*, 2007, **134**, 3-10.
37. G. C. Reyniers, G. F. Froment, F. D. Kopinke and G. Zimmermann, *Ind. Eng. Chem. Res.*, 1994, **33**, 2584-2590.
38. G. D. Stefanidis, K. M. Van Geem, G. J. Heynderickx and G. B. Marin, *Chem. Eng. J.*, 2008, **137**, 411-421.
39. G. J. Heynderickx and M. Nozawa, *Aiche J.*, 2005, **51**, 2721-2736.
40. G. D. Stefanidis, G. J. Heynderickx and G. B. Marin, *Energy Fuels*, 2006, **20**, 103-113.
41. K. M. Van Geem, M. F. Reyniers and G. B. Marin, Taking optimal advantage of feedstock flexibility with COILSIM1D, New Orleans, LA, USA, 2008.
42. D. B. Meade, B. S. Haran and R. E. White, *Mapletech*, 1996, **3**, 85-93.
43. Asian butadiene: Price analysis, <http://www.platts.com>, Accessed 12/08/2013.
44. Europe Gasoline/Naphtha-Gasoline, naphtha prices rise with oil, <http://uk.finance.yahoo.com/news/europe-gasoline-naphtha-gasoline-naphtha-175021750.html>, 2013.
45. The Jacobsen, <http://www.thejacobsen.com>, Accessed 06/06/2013, 2013.
46. Braskem, in *Business News America*.
47. M. Pearlson, Master of Science and Technology and Policy, University of Massachusetts, 2007.
48. A. J. Nizamoff, *Renewable liquids as steam cracker feedstocks*, 2010.